Kennedy, J., Ferré, T. P. A., Güntner, A., Abe, M., Creutzfeldt, B. (2014): Direct measurement of subsurface mass change using the variable baseline gravity gradient method. - *Geophysical Research Letters*, *41*, 8, p. 2827-2834.

DOI: http://doi.org/10.1002/2014GL059673

AGU PUBLICATIONS

Geophysical Research Letters

RESEARCH LETTER
10.1002/2014GL059673

Key Points:
- Variable baseline gravity gradients are measured between two or more gravimeters
- Gradient measurements eliminate ocean and atmospheric loading noise
- Infiltration rate and change in water content is estimated using gradient data

Supporting Information:
- Readme
- Figure S1
- Figure S2

Correspondence to:
J. Kennedy,
jkennedy@usgs.gov

Citation:
Kennedy, J., T. P. A. Ferré, A. Güntner, M. Abe, and B. Creutzfeldt (2014), Direct measurement of subsurface mass change using the variable baseline gravity gradient method, *Geophys. Res. Lett.*, *41*, 2827–2834, doi:10.1002/2014GL059673.

Received 20 FEB 2014
Accepted 7 APR 2014
Accepted article online 10 APR 2014
Published online 28 APR 2014

Direct measurement of subsurface mass change using the variable baseline gravity gradient method

Jeffrey Kennedy[1,2], Ty P. A. Ferré[2], Andreas Güntner[3], Maiko Abe[3], and Benjamin Creutzfeldt[4]

[1]U.S. Geological Survey, Tucson, Arizona, USA, [2]Department of Hydrology and Water Resources, University of Arizona, Tucson, Arizona, USA, [3]Helmholtz Centre Potsdam, GFZ German Research Centre for Geosciences, Potsdam, Germany, [4]Senate Department for Urban Development and the Environment, Berlin, Germany

Abstract Time-lapse gravity data provide a direct, nondestructive method to monitor mass changes at scales from centimeter to kilometer. But, the effectively infinite spatial sensitivity of gravity measurements can make it difficult to isolate the signal of interest. The variable baseline gravity gradient method, based on the difference of measurements between two gravimeters, is an alternative to the conventional approach of individually modeling all sources of mass and elevation changes. This approach can improve the signal-to-noise ratio for many applications by removing the contributions of Earth tides, loading, and other signals that have the same effect on both gravimeters. At the same time, this approach can focus the support volume within a relatively small user-defined region of the subsurface. The method is demonstrated using paired superconducting gravimeters to make for the first time a large-scale, noninvasive measurement of infiltration wetting front velocity and change in water content above the wetting front.

1. Introduction

Ground-based gravity time series have many applications, from Earth rotation dynamics [*Shirai and Fukushima*, 2001] to normal modes and other seismic phenomena [*Crossley et al.*, 2013] to basin-scale aquifer storage change [*Pool*, 2008] and soil moisture change in the critical zone [*Creutzfeldt et al.*, 2010]. This diversity exists because gravity data are sensitive to all sources of mass and elevation changes, from the local to global scale. In mass change studies, gravity change is used to measure the movement of fluids, such as the displacement of air by water during infiltration at the land surface [*Leirião et al.*, 2009], of gas by water during waterflood injection in a petroleum reservoir [*Ferguson et al.*, 2007], of water by liquid CO_2 for sequestration [*Gasperikova and Hoversten*, 2008], or the intrusion of fresh material into magma chambers [*Furuya et al.*, 2003]. All gravity mass change studies use common instrumentation, and improvements in data collection techniques and interpretation are immediately transferable. Gravity data have been used in hydrologic studies to identify hydrologic properties [*Pool and Eychaner*, 1995], to monitor artificial recharge and pumping [*Howle et al.*, 2003; *Chapman et al.*, 2008; *Gehman et al.*, 2009] and regional aquifer storage change [*Pool*, 2008; *Jacob et al.*, 2010], and to measure total water storage variations in response to long-term climate variability and extremes [*Creutzfeldt et al.*, 2010, 2012].

All time-lapse gravity investigations must isolate the signal of interest from all other sources of gravity change [*Neumeyer*, 2010]. The conventional method of removing unwanted signals is to model each source individually: Earth tides, air pressure changes, polar motion, local hydrology, and others. What remain are residuals, typically the focus of a particular study. An alternative gradient-based measurement technique, using the differenced measurement between two continuously recording gravimeters, uses common-mode differencing to remove long-wavelength effects. In doing so, processes that have essentially equal effect on both gravimeters, such as Earth tides and air pressure changes, are removed from the measurement and no longer need to be modeled individually. The remaining signal is primarily representative of a relatively small volume in close proximity to the instruments. This technique, which both improves the signal-to-noise ratio and better defines the region within which measurements are sensitive, has not previously been demonstrated in a field experiment.

Mass change studies typically require great accuracy because of the small magnitude and/or extent of mass change. Although both gravity (the first derivative of the gravitational potential in the vertical direction) and

gravity gradient (the second derivative of the potential in the *x*, *y*, or *z* direction) measurements are possible, nearly all land-based studies to date have used gravimeters (which measure gravity) because of their greater availability and lower cost as compared to gradiometers (which measure gravity gradients). Gravity gradiometry is popular for airborne and satellite (e.g., GOCE) studies because it provides improved edge detection and better signal-to-noise characteristics than gravity [*Bell*, 1998; *Jekeli and Kwon*, 1999; *Bouman and Koop*, 2004]. But, repeated airborne or satellite gradient measurements are insufficiently precise for time-lapse applications because of vehicle noise and positioning error. Terrestrial gradiometry has never been demonstrated for mass change applications in part because of the high cost of gradiometers, despite the advantages suggested by modeling exercises [*Talwani et al.*, 2001; *Reitz et al.*, 2012].

A recent field experiment at an artificial recharge facility demonstrates for the first time how the difference in gravity measured between two superconducting gravimeters provides the advantages of gravity gradiometry for mass change studies. The study presents the first large-scale, noninvasive measurement of wetting front velocity and change in water content at depths greater than a few meters. This new approach is particularly effective in isolating the signal of interest in short-duration time series data, allowing for rapid deployment applications such as during flooding or sinkhole formation, to monitor volcanic activity, or immediately following earthquakes.

2. Methods

The variable baseline gravity gradient, g_{VB}, is defined as the difference in vertical gravity between two points

$$g_{VB} = g_{z1} - g_{z2} \tag{1}$$

The term "variable baseline" is used to indicate that the measurement can be made between any two gravimeters, whether separated horizontally, vertically, or otherwise. Furthermore, the g_{VB} measurement is not normalized by the separation distance to determine Eotvos units ($1\ \mathrm{E} = 10^{-9}\ \mathrm{m/s^2/m}$) because the precision of the measurement is determined by the individual gravimeters and not the baseline distance.

2.1. Common-Mode Differencing

Common-mode differencing, which underlies the variable baseline gravity gradient approach, automatically removes the Earth tide, ocean loading, polar motion, and air pressure changes that affect both gravimeters equally. Ocean loading noise, for example, is reduced up to 5 orders of magnitude for gravimeters separated by 15 m and 3 orders of magnitude if separated by 10 km (as demonstrated by power spectra in the online supplement). The conventional approach to removing tide and ocean loading signals requires that gravimeters be deployed in a single location for a month or longer so that tide and loading models can be defined. In contrast, provided gravimeter drift is low relative to the gravity change of interest, g_{VB} data can be collected immediately and without constructing site-specific models; this makes the method especially useful for short-duration monitoring of transient events (a comparison of residual noise in short-duration, long-duration, and g_{VB} time series is presented in the supporting information). Other common-mode signals removed in the gradient measurement include land surface elevation changes, such as from local groundwater withdrawal-induced subsidence [*Wessells and Strange*, 1985; *Pool*, 2008] or from surface loading, which describes the flexure of the Earth's surface as air and water masses are redistributed at regional and global scales [*van Dam and Wahr*, 1998] and nonhydrologic subsurface mass change or uplift associated with volcanic [*Battaglia et al.*, 2008; *Charco et al.*, 2009] and tectonic [*Imanishi et al.*, 2004] activity.

Previous studies have used common-mode differencing to reduce instrumental noise but not to remove tide and other signals from continuous time series gravity data. *Bonvalot et al.* [1998] used differenced measurements to evaluate the noise level of continuously recording relative gravity meters. Differencing simultaneous measurements among instruments to remove environmental effects has been suggested for absolute gravimeter intercomparisons [*Robertson et al.*, 1996] but not to isolate tidal and loading effects. Airborne [*Jekeli*, 2006], marine [*Moody and Paik*, 2004], and satellite [*Albertella et al.*, 2002] gravity gradient measurements all use common-mode differencing to remove nongravitational effects from the instantaneous gradient measurement. Until recently, however, ground-based continuously recording gravimeters with suitably low drift (e.g., superconducting gravimeters) have not been suitable for g_{VB} measurements because each deployment required a large, purpose-built observatory [*Neumeyer*, 2010]. The prototype field enclosure

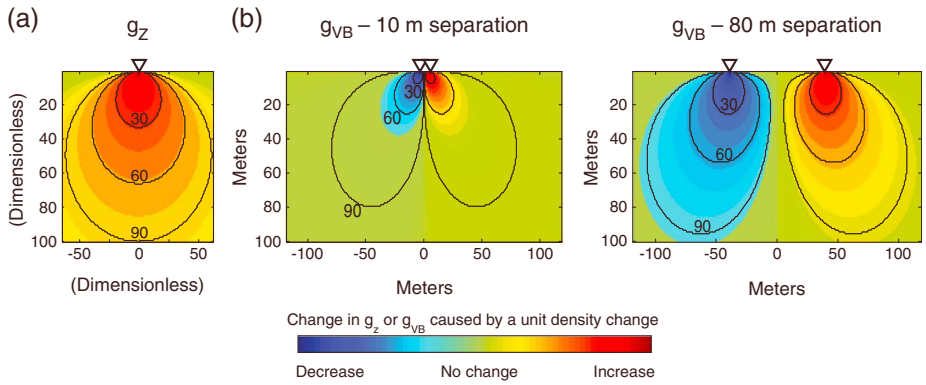

Figure 1. Sensitivity distributions showing the change in gravity caused by a unit mass change within each cell for (a) a single gravimeter and (b) two gravimeters separated horizontally by 10 m and 80 m. Triangles indicate the position of the gravimeter (s). The lines labeled 30, 60, and 90 are cumulative sensitivity contours (see text). The color bar limits are identical for all figures. These distributions are calculated assuming each cell is a prism with "infinite" extent perpendicular to the plane of the figure; as the extent of mass change in this direction decreases, measurements become relatively more sensitive to mass change at shallower depths.

used in the present study solves this problem by offering great flexibility in measurement location, and therefore, the baseline over which g_{VB} measurements are made.

The most precise gravimeters available today are superconducting gravimeters, which have precision approaching or better than 10^{-3} $(\text{nm/s}^2)^2$/mHz [*Banka and Crossley*, 1999]. The uncertainty in many different gravity effects becomes significant at this level, including tidal, ocean loading, and nutation models, spatial variations in air pressure changes, elevation changes, instrumental effects, and others [*Crossley et al.*, 2013]. Until advancements are made in modeling all of these effects, increasing instrument accuracy will not improve the signal-to-noise ratio of the residuals, which is largely determined by the magnitude of unmodeled signals. Where the variable baseline gradient method is suitable, the greatest improvement to the utility of gravity data comes from common-mode differencing using multiple gravimeters, rather than improvements in gravimeter accuracy.

2.2. The Spatial Sensitivity of Gravity and Gravity Gradient Measurements

Gravity is an integral measurement of mass at all distances. The general gravity or gravity gradient for the density distribution $\rho(\xi)$ is

$$g_{kj}(x) = \iiint \mu\rho(\xi) G_{kj}(x,\xi) dV(\xi) \tag{2}$$

where x denotes the coordinates of the gravimeter or gradiometer relative to $\rho(\xi)$, and μ is the universal gravitational constant. The spatial sensitivity of g_{kj} describes the change in gravity for a unit change in density throughout space and is denoted $G_{kj}(x,\xi)$, the gravity kernel operator. The index k indicates the potential component (x, y, or z), and j indicates the coordinate to be differentiated if g_{kj} is a gradient measurement. The vertical component of gravity measured by gravimeters is described by

$$G_z(x,\xi) = \frac{-z}{r^3} \tag{3}$$

where r is the distance between the gravimeter and $\rho(\xi)$. For the horizontal gradient (the change in the vertical gravity component in the x direction), the kernel is

$$G_{zx} = \frac{3(x_z - \xi_z)(x_x - \xi_x)}{r^5} \tag{4}$$

The gravity gradient kernel (equation (4)) decays faster with distance from the density source than does the vertical component kernel (equation (3)) and is less sensitive to more distant mass. Therefore, the support volume, defined as the region in which changes in density cause a measurable change in gravity, is smaller for a gradient measurement.

A vertical cross section through the G_z support volume is shown in Figure 1a for a single gravimeter. Each cell, or pixel, indicates the gravitational attraction due to a unit mass change of infinite horizontal extent (perpendicular

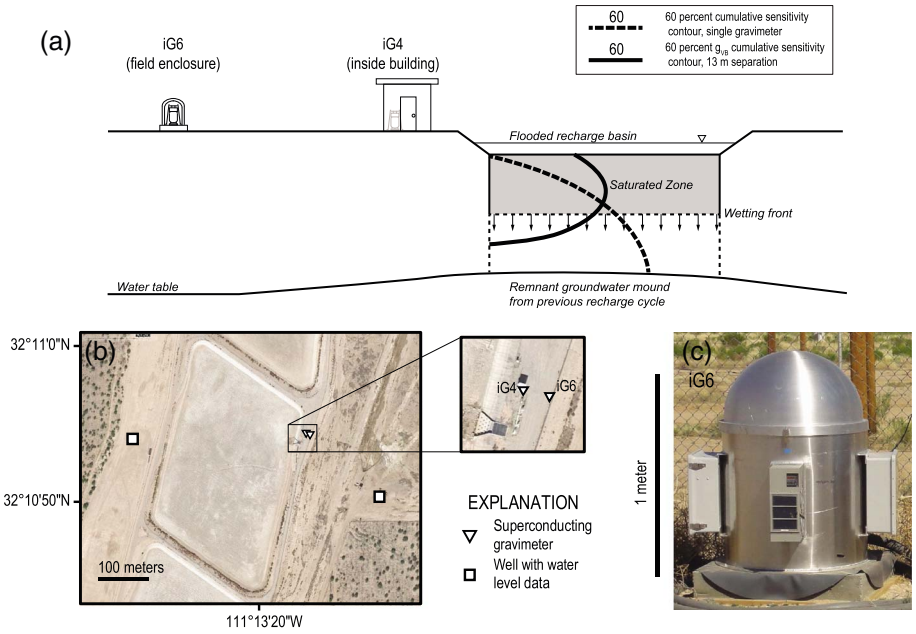

Figure 2. Configuration of the field experiment. (a) Schematic showing the location of iGrav4 and iGrav6 relative to the recharge basin and the wetting front (not to scale). Cumulative sensitivity contours (as shown in Figure 1and described in the text) are shown for the region where mass change occurs. (b) Satellite image of the study area. (c) Photograph of the prototype iGrav field enclosure.

to the page) in that cell. Similar cross sections could be constructed for mass change of shorter horizontal extent, in which case measurement sensitivity shifts toward the land surface, or other distributions, such as radially symmetric mass change.

Typically, the dimensions of the support volume of a geophysical measurement can be normalized and defined by cumulative sensitivity (CS) contours [*Ferré et al.,* 1998]. For example, the 30% CS contour would uniquely define the sample area that includes the greatest 30% of the support volume and is defined such that every prism within this volume has higher measurement sensitivity than any prism outside of this volume. The 100% contour is theoretically infinite because as sensitivity decreases away from the gravimeter, the sample volume increases. For a single gravimeter, the 90% CS contour expands to fill the domain considered, regardless of the dimensions (Figure 1a). To define the support volume in this case, a decision must be made about the extent to which mass change occurs (e.g., many hydrology studies assume no mass change below the water table). As a result, it is not strictly possible to define an appropriate support volume for a single gravimeter.

In contrast, when two gravimeters are deployed, the extent of the g_{VB} support volume and the g_{VB} CS contour locations are determined by the gravimeter separation (Figure 1b). Some cells are negative for the g_{VB} support volume because although they represent a unit mass increase, those cells are closer to and have a larger effect on the gravimeter represented by the second term of equation (1). The sensitivities of the two gravimeters become effectively equal at large distances from the midpoint of the instruments; as a result, the change in g_{VB} due to mass change at larger distances approaches zero, and the support volume is finite. Another feature of the g_{VB} measurement is that the spatial sensitivity, and therefore the location of the CS contours, can be modified intentionally by changing the gravimeter separation: decreasing the separation focuses the measurements to shallower depths and smaller extent. The support volume of a g_{VB} measurement can be defined a priori and will remain fixed throughout a survey because the local measurement sensitivity does not depend on the distribution of the property of interest (e.g., density) within the subsurface. This characteristic of gravity is unique among hydrogeophysical methods.

2.3. Experimental Design, Data Processing, and Hydrologic Model

To test the applicability of g_{VB} measurements for mass change applications, a field experiment was conducted at an artificial recharge facility near Tucson, Arizona, USA. Two iGrav® superconducting gravimeters

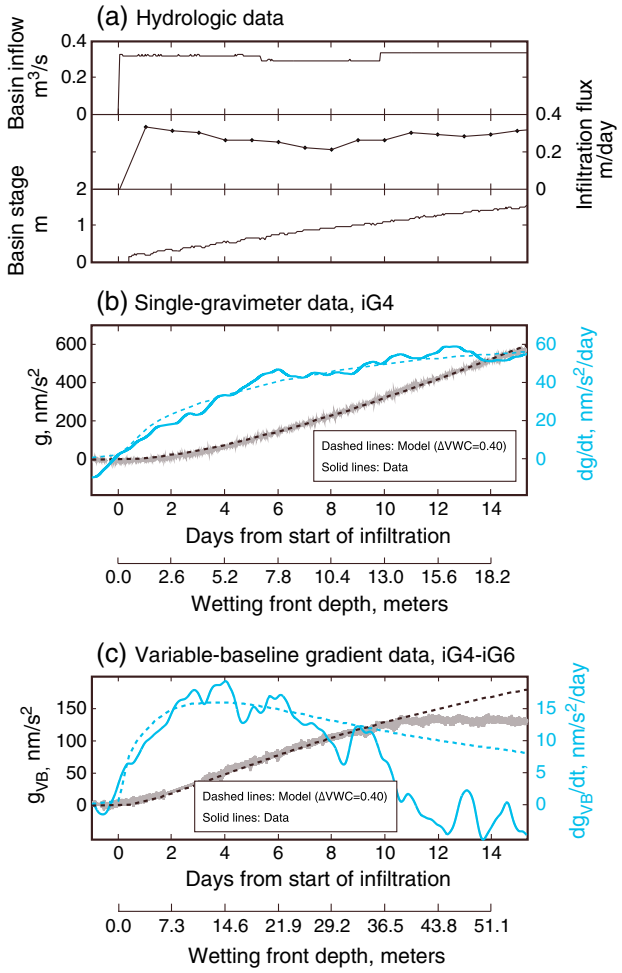

Figure 3. Measured (a) hydrologic and (b and c) gravity data during an artificial recharge experiment. Infiltration flux is calculated from basin inflow, volume, and stage data. Gravity data (Figures 3b and 3c) are presented both as cumulative change (black lines) and as rate of change (blue lines). The relation between the two horizontal scales in Figures 3b and 3c are determined based on the wetting front velocity that minimizes root-mean-square error (RMSE) for the respective measurement.

(GWR Instruments, Inc., meter numbers iG4 and iG6; mention of a particular trade name does not imply endorsement by the U.S. Government) were located 16 and 29 m from the edge of a 265 m × 315 m (83,130 m^2) recharge (i.e., infiltration) basin, about 3.8 m above the average elevation of the basin floor (Figure 2). Gravimeter iG6 was installed in a prototype field enclosure with a 1 m × 1 m footprint—a quickly deployable design that allows short-duration experiments for which g_{VB} measurements are most effective. Gravimeter iG4 was installed in a small building housing control equipment. The basin was flooded starting at 22:00 UTC on 7 December 2012, with a continuous inflow rate of about 0.3 m^3/s for 75 days (Figure 3a). Inflow was measured in the delivery pipe using an ultrasonic flowmeter, and water levels in the basin and in several nearby wells were recorded hourly using electronic pressure transducers. Land surface elevation changes during the experiment measured using continuous GPS data near iG4 were imperceptible and no greater than 1 cm.

For comparison with g_{VB} measurements, single-gravimeter residuals were calculated for iG4 using a site-specific tide model parameterized using 15 months of data from iG4 and BAYTAP-G software [*Tamura et al.*, 1991]. The admittance factor for air pressure changes, −3.26 nm/s^2/hPa, was determined by regression. Gravity data were decimated from 1 s to 60 s using linear interpolation and a 0.5 Hz low-pass filter [*Van Camp and Vauterin*, 2005], and a LOWESS (locally weighted scatterplot smoothing) curve calculated for the time derivative of the residuals shown in Figures 3b and 3c to reduce noise introduced by differentiating. A relatively wide LOWESS span of 2000 was required due to a diurnal signal in the iG6 data caused by sensitivity to uncompensated temperature changes in the prototype field enclosure. The gravitational attraction of water ponded in the basin (as opposed to in the subsurface) was removed from g and g_{VB} measurements using a modeled stage gravity relationship based on the basin topography. No instrumental drift correction was made. Measurements using an FG5 absolute gravimeter (Micro-g LaCoste, Inc.) in March and June 2012 established that the observed instrumental trend of both iGrav gravimeters (iG6 was installed at a nearby location) was less than the measurement precision, about 20 nm/s^2, during that 3 month period. The maximum probable instrumental drift rate—tens of nm/s^2/year—is much less than the hydrology-induced gravity change of tens of nm/s^2/d (Figures 3b and 3c).

Gravity data are used with an infiltration model to determine infiltration rate, wetting front velocity, and change in water content. Infiltration is modeled as vertical flow with a sharp wetting front (i.e., piston flow); assuming constant infiltration rate and uniform initial water content, the wetting front moves with constant velocity. In part, these assumptions are justified because of the relatively large, rapidly developed ponded head

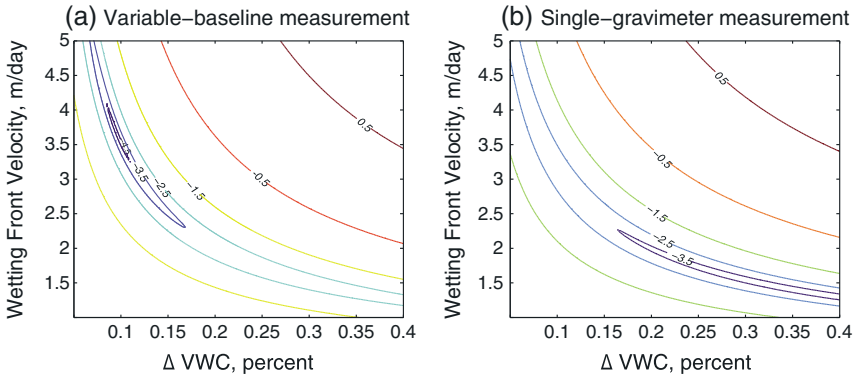

Figure 4. Response surface showing *log* (normalized RMSE), calculated as the difference between (a) g_{VB} or (b) single-gravimeter data and predicted gravity using a 1-D, piston flow infiltration model.

in the basin (Figure 3a), which would quickly overwhelm early stage, capillary-driven infiltration. Furthermore, the basin was dry for 90 days prior to the experiment, creating a subsurface with relatively homogeneous initial water content. Evaporation is very low compared to infiltration. Under these conditions, the infiltration rate i is related to the change in volumetric water content ΔVWC and the wetting front velocity, v_{wf}

$$i = v_{wf}\Delta\mathrm{VWC} \tag{4}$$

The change in gravity during infiltration is calculated for each wetting front depth by summing the gravitational attraction of 1 m × 1 m prisms beneath the recharge basin [*Nagy*, 1966]. The top of each prism is the elevation of the recharge basin for that cell, and the bottom is the wetting front depth.

3. Hydrological Interpretation of the g_{VB} Measurement

During infiltration, mass change initially occurs close to the ground surface, at nearly the same level as the instrument (Figure 2a), which results in small changes in the vertical component of gravity. As the wetting front depth increases, measurement sensitivity increases, and there will be an initial increase in the rate of change of the vertical gravity component. Over time, however, the increasing distance to mass change at the wetting front results in a decrease in the rate of gravity change. The resulting maximum sensitivity provides information about the movement of the wetting front because it represents a time and location of the wetting front at which the gravity kernel G (equation (2)) is known. For the spatial configuration of gravimeters and mass change in this example, at the time (3.9 days) and depth (13.0 m) of maximum sensitivity of the g_{VB} measurement (Figure 3c), the right-hand side of equation (1) is equivalent to 47.6 nm/s^2/m; this is the gravity change that would be caused by 1 m of pure water at this depth. In contrast, the single-gravimeter dg/dt data increase gradually with depth, not reaching a maximum value (and therefore a known depth) until nearly 50 m depth (beyond the upper x axis limit of Figure 3b), and G is poorly defined for any particular wetting front depth. Finally, there is a distinct transition in the dg_{VB}/dt data after about 10 days (Figure 3c) that gives a clear indication that infiltrated water has reached the water table and is spreading laterally at depth, moving more directly beneath the gravimeters, and causing both to respond nearly equally as the water table rises. The model deviates from the observed data at this time because it includes only vertical infiltration below the basin and not groundwater mounding or lateral flow. This change is not evident in the single-gravimeter data (Figure 3b).

This difference in "identifiability" of G leads to differences in the identifiability of i, v_{wf}, and ΔVWC. The role of v_{wf} is to define the relation between the incremental change in gravity with depth determined from the infiltration model (Figures 3b and 3c, dashed lines) and the measured rates of change of gravity and gravity gradient, dg/dt and dg_{VB}/dt (solid lines). That is, it determines the scaling between the horizontal time and depth axes of Figures 3b and 3c and converts the change in gravity with depth predicted from the infiltration model to change in gravity with time. The change in water content ΔVWC determines the position of each gravity curve on the y axis. Considering the first 10 days of data, response surfaces of the natural log of the root-mean-square error (calculated as the infiltration-model-predicted gravity change minus the observed gravity data), normalized by the range of either g or g_{VB}, respectively, give an optimal value near v_{wf} = 3.6 m/d and ΔVWC = 0.09 for the g_{VB} data (Figure 4a) and an optimal value near v_{wf} = 1.3 m/d and ΔVWC = 0.4 for the

single-gravimeter data at iG4 (Figure 4b). The g_{VB} data better constrain both parameters, whereas the single-gravimeter data are largely insensitive to wetting front velocity in the region where ΔVWC is optimal. That is, the optimal single-gravimeter solution is only slightly better than many other solutions, including the optimal variable baseline solution; the optimal variable baseline solution is much better than any other solution. The optimum parameter estimates of the two measurements differ widely, but both simulate the data reasonably well during the first 10 days of infiltration, when the piston flow infiltration model (which does not simulate groundwater mounding) is appropriate (Figures 3b and 3c).

Hydrologic data provide independent information for evaluating the gravity-estimated parameters. From basin inflow and stage data, i can be calculated; during the first 9 days, the average infiltration rate is 0.29 m/d (Figure 3a), in good agreement with the 0.32 m/d infiltration rate estimated from equation (4) using g_{VB} data, but much less than the 0.52 m/d infiltration rate estimated using single-gravimeter data. The travel time of infiltrated water through the unsaturated zone can be determined from the depth to water beneath the basin prior to the experiment, estimated to be 55 m ± 10 m based on two wells with depths to water relative to the bottom of the basin of 70.7 m and 69.1 m located 82 and 145 m from the recharge basin, respectively. The water level under the basin is assumed to be slightly higher than in the wells because of a dissipating groundwater mound from a previous recharge cycle. Because of the relatively thick unsaturated zone and the indication from the dg_{VB}/dt data that the wetting front reaches the water table after 10 days (Figure 3c), the v_{wf} estimate from single-gravimeter data (1.3 m/d) appears to be much too low; v_{wf} estimated using g_{VB} data (3.6 m/d) is closer, but still too low, indicating that the height of the groundwater mound is underestimated or v_{wf} increases with depth. Finally, water levels at the closest well, 82 m from the basin, start to increase 20 days after the basin is first flooded, providing further indication of the rapid transport of water as indicated by g_{VB} data.

In summary, the advantages of g_{VB} over g_z for this example are (1) the velocity of the wetting front can be identified earlier and at shallower depths, and the transition from vertical infiltration to horizontal spreading at the water table is obvious; (2) the depth at which the wetting front velocity is determined with greatest precision can be selected in advance by varying the gravimeter positions; and (3) the wetting front velocity and the change in water content are better resolved.

4. Discussion

Although a relatively simple, illustrative case study, these results can be related to other applications because the need to isolate the signal of interest from other signals is ubiquitous for all time-lapse gravity studies. Immediate possibilities for g_{VB} measurements are to identify mass change from volcanic deflation-inflation events and near-surface lava reservoirs, preseismic and coseismic mass change, to locate the water table relative to the root zone in riparian areas or to noninvasively monitor water flux through subsurface contamination isolation facilities. The noise reduction offered by common-mode differencing is particularly valuable when gravimeters are deployed at a new site for the first time and makes possible rapid deployments to capture transient phenomena. While g_{VB} was interpreted using a simple infiltration model to determine i, v_{wf}, and ΔVWC in the example presented here, a similar improvement in the ability to resolve near-surface mass change would be expected if the data were used for more complex geophysical inversion or with a parameter estimation software tool such as PEST [*Doherty et al.*, 2010].

The obvious evolution of g_{VB} measurements is toward networks of continuously recording gravimeters. Such networks have been suggested for volcanic monitoring [*Crossley and Hinderer*, 2005; *Williams-Jones et al.*, 2008], including the use of common-mode differencing to reduce noise [*Bonvalot et al.*, 1998]. Similarly, networks of continuous gravimeters have been used to monitor seismic-induced mass change [*Imanishi et al.*, 2004] and continental water storage [*Crossley et al.*, 2005; *Kang et al.*, 2011], but the study presented here is the first to have collected and interpreted the differenced measurement between two or more gravimeters to study local hydrology (or other mass change) at a single site. In the foreseeable future, continuous gravity measurements in a borehole will be possible, further expanding the applications of g_{VB} measurements toward true 4-D gravimetry.

Acknowledgments

Research was supported by the USGS Groundwater Resources Program, NSF grant EAR-1246619, and the Arizona Water, Environmental, and Energy Solutions program. Data collected under these programs are available from the corresponding author. GWR Instruments, Inc. is gratefully acknowledged for loaning one gravimeter and the prototype field enclosure. Assistance with FG5 measurements from Dan Winester, NOAA-National Geodetic Survey, is gratefully acknowledged, as are many helpful comments from Donald Pool, Bruce Gungle, David Crossley, and an anonymous reviewer. The ocean loading service provided by Hans-Georg Scherneck was used to calculate nao99.b tidal parameters.

The Editor thanks David Crossley and an anonymous reviewer for their assistance in evaluating this paper.

References

Albertella, A., F. Migliaccio, and F. Sansó (2002), Goce: The earth gravity field by space gradiometry, *Celest. Mech. Dyn. Astron.*, *82*(1-4), 1–15.

Banka, D., and D. Crossley (1999), Noise levels of superconducting gravimeters at seismic frequencies, *Geophys. J. Int.*, *139*(1), 87–97, doi:10.1046/j.1365-246X.1999.00913.x.

Battaglia, M., J. Gottsmann, D. Carbone, and J. Fernández (2008), 4D volcano gravimetry, *Geophysics*, *73*(6), WA3–WA18. [Available at http://geophysics.geoscienceworld.org/content/73/6/WA3.]
Bell, R. E. (1998), Gravity Gradiometry, *Sci. Am.*, *278*, 74–79.
Bonvalot, S., M. Diament, and G. Gabalda (1998), Continuous gravity recording with Scintrex CG-3 M meters: A promising tool for monitoring active zones, *Geophys. J. Int.*, *135*(2), 470–494, doi:10.1046/j.1365-246X.1998.00653.x.
Bouman, J., and R. Koop (2004), Gravity gradients and spherical harmonics - a need for different GOCE products?, in *Proc. Second International GOCE User Workshop "GOCE, The Geoid and Oceanography", ESA-ESRIN*, Frascati, Italy, 8–10 March 2004, Eur. Space Agency Spec. Publ., ESA SP-569, 6 pp.
Chapman, D. S., E. Sahm, and P. Gettings (2008), Monitoring aquifer recharge using repeated high-precision gravity measurements: A pilot study in South Weber, Utah, *Geophysics*, *73*(6), WA83–WA93.
Charco, M., A. G. Camacho, K. F. Tiampo, and J. Fernández (2009), Spatiotemporal gravity changes on volcanoes: Assessing the importance of topography, *Geophys. Res. Lett.*, *36*, L08306, doi:10.1029/2009GL037160.
Creutzfeldt, B., A. Güntner, S. Vorogushyn, and B. Merz (2010), The benefits of gravimeter observations for modelling water storage changes at the field scale, *Hydrol. Earth Syst. Sci.*, *14*(9), 1715–1730, doi:10.5194/hess-14-1715-2010.
Creutzfeldt, B., T. P. A. Ferré, P. Troch, B. Merz, H. Wziontek, and A. Güntner (2012), Total water storage dynamics in response to climate variability and extremes: Inference from long-term terrestrial gravity measurement, *J. Geophys. Res.*, *117*, D08112, doi:10.1029/2011JD016472.
Crossley, D., and J. Hinderer (2005), Using SG arrays for hydrology in comparison with GRACE satellite data, with extension to seismic and volcanic hazards, *Korean J. Remote Sens.*, *21*(1), 31–49.
Crossley, D., J. Hinderer, and J.-P. Boy (2005), Time variation of the European gravity field from superconducting gravimeters, *Geophys. J. Int.*, *161*(2), 257–264, doi:10.1111/j.1365-246X.2005.02586.x.
Crossley, D., J. Hinderer, and U. Riccardi (2013), The measurement of surface gravity, *Rep. Prog. Phys.*, *76*(4), 046,101, doi:10.1088/0034-4885/76/4/046101.
Doherty, J., R. J. Hunt, and M. J. Tonkin (2010), Approaches to highly parameterized inversion: A guide to using PEST for model-parameter and predictive-uncertainty analysis, *U.S. Geol. Surv. Sci. Investig. Rep. 2010 – 5211*, 71 pp. [Available at http://pubs.usgs.gov/sir/2010/5211.]
Ferguson, J., T. Chen, J. L. Brady, C. L. V. Aiken, and J. E. Seibert (2007), The 4D microgravity method for waterflood surveillance II — Gravity measurements for the Prudhoe Bay reservoir, Alaska, *Geophysics*, *72*(2), I33–I43.
Ferré, T. P. A., J. H. Knight, D. L. Rudolph, and R. G. Kachanoski (1998), The sample area of conventional and alternative time domain reflectometry probes, *Water Resour. Res.*, *34*(11), 2971–2979.
Furuya, M., S. Okubo, W. Sun, Y. Tanaka, J. Oikawa, H. Watanabe, and T. Maekawa (2003), Spatiotemporal gravity changes at Miyakejima Volcano, Japan: Caldera collapse, explosive eruptions and magma movement, *J. Geophys. Res.*, *108*(B4), 2219, doi:10.1029/2002JB001989.
Gasperikova, E., and G. M. Hoversten (2008), Gravity monitoring of CO2 movement during sequestration: Model studies, *Geophysics*, *73*(6), WA105–WA112.
Gehman, C. L., D. L. Harry, W. E. Sanford, J. D. Stednick, and N. A. Beckman (2009), Estimating specific yield and storage change in an unconfined aquifer using temporal gravity surveys, *Water Resour. Res.*, *45*, W00D21, doi:10.1029/2007WR006096.
Howle, J. F., S. P. Phillips, R. P. Denlinger, and L. F. Metzger (2003), Determination of specific yield and water-table changes using temporal micro-gravity surveys collected during the second injection, storage, and recovery test at lancaster, Antelope Valley, California, November 1996 through April 1997, U.S. Geol. Surv. Water-Resources Investig. Rep. *03-4019*, 28.
Imanishi, Y., T. Sato, T. Higashi, W. Sun, and S. Okubo (2004), A network of superconducting gravimeters detects submicrogal coseismic gravity changes, *Science*, *306*(5695), 476–8, doi:10.1126/science.1101875.
Jacob, T., R. Bayer, J. Chery, N. Le Moigne, and N. Le Moigne (2010), Time-lapse microgravity surveys reveal water storage heterogeneity of a karst aquifer, *J. Geophys. Res.*, *115*(B6), 1–18, doi:10.1029/2009JB006616.
Jekeli, C. (2006), Airborne Gradiometry Error Analysis, *Surv. Geophys.*, *27*(2), 257–275, doi:10.1007/s10712-005-3826-4.
Jekeli, C., and J. H. Kwon (1999), Results of airborne vector (3-d) gravimetry, *Geophys. Res. Lett.*, *26*(23), 3533–3536.
Kang, K., H. Li, and P. Peng (2011), Seasonal variations in hydrological influences on gravity measurements using gPhones, *Terr. Atmos. Ocean. Sci.*, *22*(2), 1–12, doi:10.3319/TAO.2010.08.02.01(TibXS).
Leirião, S., X. He, L. Christiansen, O. B. Andersen, and P. Bauer-Gottwein (2009), Calculation of the temporal gravity variation from spatially variable water storage change in soils and aquifers, *J. Hydrol.*, *365*(3-4), 302–309, doi:10.1016/j.jhydrol.2008.11.040.
Moody, M. V., and H. J. Paik (2004), A Superconducting Gravity Gradiometer for inertial navigation, in *PLANS 2004. Position Location and Navigation Symposium (IEEE Cat. No.04CH37556)*, pp. 775–781, Ieee.
Nagy, D. (1966), The gravitational attraction of a right rectangular prism, *Geophysics*, *31*(2), 362–371.
Neumeyer, J. (2010), Superconducting Gravimetry, in *Sciences of Geodesy - I*, pp. 339–413, Springer, Heidelberg, Dordrecht, London, and New York.
Pool, D. R. (2008), The utility of gravity and water-level monitoring at alluvial aquifer wells in southern Arizona, *Geophysics*, *73*(6), WA49–WA59.
Pool, D. R., and J. H. Eychaner (1995), Measurements of aquifer-storage change and specific yield using gravity surveys, *Ground Water*, *33*(3), 425–432.
Reitz, A., R. A. Krahenbuhl, Y. Li, and D. DiFrancesco (2012), Feasibility analysis of time-lapse gravity gradiometry for reservoir monitoring, in *SEG Las Vegas 2012 Annual Meeting*, pp. 1–5.
Robertson, D., G. Sasagawa, and F. Klopping (1996), The use of differencing to eliminate environmental effects in the intercomparison of absolute gravity meters, *Geophys. Res. Lett.*, *23*(3), 245–248.
Shirai, T., and T. Fukushima (2001), Detection of excitations of free core nutation of the Earth and their concurrence with huge Earthquakes, *Geophys. Res. Lett.*, *28*(18), 3553–3556.
Talwani, M., D. DiFrancesco, and W. Feldmand (2001), System enables time-lapse gradiometry, *Am. Oil Gas Rep*, *44*, 101–108.
Tamura, Y., T. Sato, M. Ooe, and M. Ishiguro (1991), A procedure for tidal analysis with a Bayesian information criterion, *Geophys. J. Int.*, *104*, 507–516, doi:10.1111/j.1365-246X.1991.tb05697.x.
Van Camp, M., and P. Vauterin (2005), Tsoft: Graphical and interactive software for the analysis of time series and Earth tides, *Comput. Geosci.*, *31*(5), 631–640, doi:10.1016/j.cageo.2004.11.015.
Van Dam, T., and J. Wahr (1998), Modeling environment loading effects: A review, *Phys. Chem. Earth*, *23*(9-10), 1077–1087.
Wessells, C. W., and E. Strange (1985), Results of repeat gravity measurements in areas of ground water withdrawal subsidence, *Eos Washington D. C.*, *66*(18), 364.
Williams-Jones, G., H. Rymer, G. Mauri, J. Gottsmann, M. Poland, and D. Carbone (2008), Toward continuous 4D microgravity monitoring of volcanoes, *Geophysics*, *73*(6), WA19–WA28.